Simultaneous CCD Photometry of Two Eclipsing Binary Stars in Pegasus—Part 2: BX Pegasi

Kevin B. Alton
UnderOak Observatory, 70 Summit Avenue, Cedar Knolls, NJ 07927; kbalton@optonline.net

Received December 5, 2012; revised January 3, 2013; accepted January 3, 2013

Abstract BX Peg is an overcontact W UMa binary system (P = 0.280416 d) which has been rather well studied, but not fully understood due to complex changes in eclipse timings and light curve variations attributed to star spots. Photometric data collected in three bandpasses (B, V, and I_c) produced nineteen new times of minimum for BX Peg. These were used to update the linear ephemeris and further analyze potential changes in orbital periodicity by examining long-term changes in eclipse timings. In addition, synthetic fitting of light curves by Roche modeling was accomplished with the assistance of three different programs, two of which employ the Wilson-Devinney code. Different spotted solutions were necessary to achieve the best Roche model fits for BX Peg light curves collected in 2008 and 2011. Overall, the long-term decrease (9.66×10^{-3} sec y^{-1}) in orbital period defined by the parabolic fit of eclipse timing data could arise from mass transfer or angular momentum loss. The remaining residuals from observed minus predicted eclipse timings for BX Peg exhibit complex but non-random behavior. These may be related to magnetic activity cycles and/or the presence of an unseen mass influencing the times of minimum, however, additional minima need to be collected over a much longer timescale to resolve the nature of these complex changes.

1. Introduction

The variable behavior of BX Peg was first discovered by Shapley and Hughes (1934) and thereafter studied by numerous investigators. Briefly, BX Peg belongs to the W UMa class of eclipsing binaries whose component main sequence stars (spectral type A–F to early K) rotate rapidly (P < 1 day) while in contact with each other. The spectral type of this overcontact binary has been variously assigned between G4V and G9V. Light curves and/or refined photoelectric- or CCD-derived light elements for BX Peg have been reported by Zhai and Zhang (1979), Hoffmann (1982), Kaluzny (1984), Samec (1990), Leung *et al.* (1985), Samec and Bookmyer (1987), De Young *et al.* (1991), Samec and Hube (1991), Lee *et al.* (2004), and Lee *et al.* (2009). A radial velocity study (Samec and Hube 1991) yielded a spectroscopic mass ratio value ($q_{sp} = 0.372$); based solely upon these data, BX Peg belongs to the W-type classification where the smaller secondary is somewhat hotter than the more

massive primary star. This system also exhibits asymmetry at maximum light which is ascribed to the so-called O'Connell effect frequently observed with W UMa variables. Only the photoelectric V-band light curve collected in 1979 (Hoffmann 1982) and the 1978 B-band curve produced by Zhai and Zhang (1979) convincingly exhibited a positive O'Connell effect (Max I > Max II). Aside from a few examples where Max I ≈ Max II (Samec and Bookmyer 1987), the majority of the published light curves show a negative O'Connell effect (Max II > Max I). In most cases investigators invoked the addition of cool or hot starspots in order to obtain the best light curve fits with Roche modeling. The high orbital inclination angle (i ~88°) indicates that our view of this eclipsing binary is very close to edge-on.

2. Observations and data reduction

Session dates in 2008 and 2011, along with the photometric equipment, acquisition parameters, and image processing, were exactly as described in the companion paper (Part I; Alton 2013) for KW Peg, which is in the same field-of-view (FOV) as BX Peg.

Roche-type modeling was performed using BINARY MAKER 3 (BM3; Bradstreet and Steelman 2002), WDWINT v5.6a (Nelson 2009), and PHOEBE v.31a (Prša and Zwitter 2005), the latter two of which employ the Wilson-Devinney (W-D) code (Wilson and Devinney 1971; Wilson 1979). 3-D spatial renderings of BX Peg were also produced by BM3 once each model fit was finalized. Times of minimum (ToM) were estimated using the method of Kwee and van Woerden (1956) as implemented in Minima V25c (Nelson 2007).

3. Results and discussion

3.1. Photometry

Five stars in the same FOV as BX Peg were used to derive catalogue-based (MPOSC3) magnitudes in MPO CANOPUS (Minor Planet Observer 2010; Table 1). Comparison stars showed no evidence of inherent variability over the period of image acquisition and stayed within ±0.015 magnitude for V and I_c filters and ±0.03 for the B passband.

3.2. Ephemerides

3.2.1. Light curves from 2008 Campaign

Photometric values in B (n = 873), V (n = 863), and I_c (n = 885) were folded by filter to produce light curves that spanned 23 days in October 2008 (Figure 1). These determinations produced eight new ToM values in each bandpass. No meaningful color dependencies emerged; therefore the timings from all three filters were averaged for each session (Table 2). The Fourier routine (FALC) in MPO CANOPUS provided a period solution for all the data after

initially seeding the analysis with the orbital period derived by Kreiner (2004). The corresponding linear ephemeris (Equation 1) was determined as follows using the latest primary epoch from this dataset:

$$\text{Min. I (hel.)} = 2454770.5181\ (8) + 0.2804259\ (1)\ E \quad (1)$$

3.2.2. Light curves from 2011 Campaign

Photometric values in B (n = 638), V (n = 646), and I_c (n = 649) were folded by filter to produce light curves that spanned 32 days (Figure 2) in October and November 2011. These observations produced eleven new ToM values in each bandpass (Table 2). As described above for the 2008 data, the linear ephemeris (Equation 2) for the last primary epoch captured in 2011 was as follows:

$$\text{Min. I (hel.)} = 2455868.6282\ (8) + 0.2804197\ (1)\ E \quad (2)$$

The overall accuracy of the orbital period can be improved by pooling the light curve data from 2008 and 2011 which extends the time baseline for Fourier analysis from less than 33 days to 1,126 days. As a result, the composite linear ephemeris (Equation 3) was determined to be:

$$\text{Min. I (hel.)} = 2455868.6282\ (8) + 0.2804164\ (5)\ E \quad (3)$$

which compares more favorably with values reported over the past five decades. As is standard practice at UnderOak Observatory (UO), all period determinations were independently confirmed using PERANSO v2.5 (CBA Belgium Observatory 2011) by applying periodic orthogonals (Schwarzenberg-Czerny 1996) to fit observations and analysis of variance (ANOVA) to evaluate fit quality. In toto, eleven new secondary (s) and eight primary (p) minima were recorded during this investigation of BX Peg. These nineteen new minima along with published values starting in 1960 (Table 3) were used to assess eclipse timing (ET) over the past fifty-one years. The reference epoch (Kreiner 2004) employed for calculating ET residuals (ETR) was defined by the following linear ephemeris (Equation 4):

$$\text{Min. I (hel.)} = 2452500.2563\ (8) + 0.2804177\ (2)\ E \quad (4)$$

To visualize the progression of orbital periodicity over time the difference between the observed eclipse times and those predicted by the reference epoch are plotted against period cycle number (Figure 3). Although commonly called an observed minus computed, or O–C diagram, this generalized term fails to exactly inform the reader about which variables are being plotted. Going forward, the term ET diagram will be used instead. The top panel in Figure 3 chronicles a very complex pattern of eclipse timings for BX Peg over the past fifty-one years. Collectively all of the ETR values describe a parabola as a function of time, however, there is significant scatter which complicates any cogent interpretation about the periodic behavior of this system. Due to the very

apparent variability associated with visual (vis) and photographic (pg) values, photoelectric- (PE) and CCD-derived observations were weighted eight-fold while curve fitting. As indicated by the downwardly turned parabolic relationship ($c + a_1x - a_2x^2$) between ETR and time, the corresponding period decrease is similar irrespective of whether all data (Figure 3, top) or just the CCD/PE data are evaluated (Figure 3, middle). This leads to an updated quadratic ephemeris (Equation 5) as follows:

$$\text{Min. I (hel.)} = 2455873.4019\ (4) + 0.28041753\ (4)\ E - 4.29\ (17) \times 10^{-11}\ E^2 \quad (5)$$

In this case the orbital period rate of decrease ($\Delta p/p = 2a_2 = 8.585 \pm 0.169 \times 10^{-11}$) of this system, which is equivalent to a period decrease rate of $dP/dt = +0.00966$ sec y^{-1}, has lasted from at least 1960. The secular, or long-term period change associated with a parabola-shaped ET diagram is often attributed to mass transfer or by angular momentum loss (AML) due to magnetic stellar wind. The first systematic examination of period and light variations for BX Peg was conducted by Lee *et al.* (2004) and included ET data up through mid-2003 (cycle 1124). Essentially their analysis suggests the continuous period decrease is most likely related to mass transfer from the primary to secondary star or a combination of AML and mass transfer. Quadratic residuals derived from the CCD and PE data (Figure 3, bottom) reveal a potential quasi-sinusoidal change up through 2003 as described by Lee *et al.* (2004). Thereafter, new eclipse timings reveal what appears to additional cyclic changes of shorter duration. Further attempts to mathematically model all the CCD and PE eclipse timing data using non-linear polynomial regression with and without a sine term did not lead to a good fit of the data. Cyclic changes of eclipse timings are also attributed to the light-time effect of a third unseen body and/or cyclical changes in the magnetic activity of either binary constituent. Beyond speculation there presently are not enough supporting data which could be used to confidently explain the complex behavior of this binary system.

A near-term linear ephemeris (Equation 6) from the present investigation was projected from a straight line segment (Figure 3, middle inset) covering observations from 2008 to 2011; calculated least-squares fit residuals over this period of time are provided in Table 4.

$$\text{Min. I (hel.)} = 2455873.3958\ (8) + 0.28041636\ (8)\ E \quad (6)$$

Not surprisingly, this near term orbital period is consistent with the linear ephemeris (Equation 3) determined directly from Fourier analysis of the pooled (2008 and 2011) light curves. Given the complex changes in orbital period for this system, revised ephemerides for BX Peg should be determined on a regular basis to maintain an accurate record about the behavior of this overcontact variable system.

3.3. Light curve behavior

Individual light curves from 2008 (Figure 1) and 2011 (Figure 2) show that minima are separated by 0.5 phase and as might be expected from a contact binary system, are consistent with a circular orbit. Similar to most published light curves for BX Peg (Samec 1990, De Young *et al.* 1991, Lee *et al.* 2004, and Lee *et al.* 2009), a negative, albeit modest O'Connell effect (Max I fainter than Max II) was observed with all passbands during the 2008 campaign. The so-called O'Connell effect is believed to involve the presence of cool starspot(s), hot regions, gas stream impact on one or both of the binary components, and/or other unknown phenomena which distort surface homogeneity and can produce unequal heights during quadrature (Yakut and Eggleton 2005). In 2008 this asymmetry was most noticeable in B-band. By comparison the 2011 light curves exhibited a positive (Max I brighter than Max II) O'Connell effect but in this case the asymmetry was more prominent in V-band (Table 5). Brighter measurements during first quadrature (Max I) had only been sporadically reported (Hoffmann 1982; Zhai and Zhang 1979) in the past.

3.4. Spectral classification

The effective temperature (Teff) of the primary was estimated from the mean observed color index (B–V = 0.716) determined during quadrature (0.25 P and 0.75 P) in 2008 and 2011. Since W UMa systems are invariably comprised of main sequence stars, this corresponds to the effective temperature (5613 K) associated with spectral class G7V (Flower 1996; Harmanec 1988). Similarly, other investigators (Kaluzny 1984, Samec 1990, Samec and Hube 1991, Leung *et al.* 1985, Maceroni and van't Veer 1996, Lee *et al.* 2004, and Lee *et al.* 2009) report that BX Peg ranges between G4 (5807 K) and G9V (5330 K). Supporting color index (B–V) data from other surveys (Table 6) indicate a system ranging between G3 and G9V. For Roche modeling, the average Teff (5520 K; G7-G8V) from this tabulation was adopted for the more massive but cooler star. Assignment of this temperature to the cooler component in a W-type W UMa variable at first glance seemed counter-intuitive. Although the luminosity of a star is proportional to the fourth power of its effective temperature according to the Stefan-Boltzmann law ($L = 4\pi R^2 \alpha T^4$), brightness also increases with surface area or radius squared (R^2). As is the case with most W UMa type variable stars, the temperature difference between each main sequence component rarely exceeds 500 K. It follows that the overall luminosity of BX Peg is dominated by the nearly three-fold mass difference between the primary and secondary components, which, according to the mass-radius relationship ($R = M^{0.8}$) for main sequence stars, also corresponds to more than a two-fold difference in size. A heads-up comparison from a 500 K difference in temperature $(6020/5520)^4$ versus the putative radius ratio $(1/0.38)^{0.8}$ from radial velocity data reveals that overall luminosity increases 1.4-fold with a hotter secondary but by a greater amount (2.2-fold) due to the increased size of the primary. This "size-beats-

temperature-difference" luminosity relationship for BX Peg is confirmed in the next section where the relevant attributes ($Teff_1$, $Teff_2$, R_1, and R_2) for this binary system are defined in more detail after Roche modeling.

3.5. Roche Modeling

3.5.1. 2008 Light Curves

Coincidently, Lee *et al.* (2009) also recorded light curve data (B-, V-, and R_c-band) for BX Peg in the fall of 2008. Different starspots were used by these investigators to model data collected between September 27 and October 22 (Group 1; Max I < Max II) and on two consecutive nights (15th and 16th) in November (Group 2; Max I > Max II). Group 1 data were fit with a single cool spot on the more massive star, whereas Group 2 also required a hot spot on either star. Since the 2008 data collected at UO only included values from October, a photometric solution using PHOEBE was initially attempted by adopting all of the parameters described for Group 1 (Lee *et al.* 2009). Roche modeling proceeded with phased B-, V-, and I_c-band data which had been transformed into catalogue-based magnitudes. Mode 3 (an overcontact binary system not in thermal contact) with synchronous rotation and circular orbits were employed in PHOEBE. Each model fit of data from the present study incorporated individual observations assigned an equal weight of 1. All Group 1 parameters from Lee *et al.* (2009) remained fixed whereas phase shift and passband specific luminosity corrections were iteratively adjusted using differential corrections (DC) to achieve a simultaneous minimum residual fit of all (B, V, and I_c) photometric observations. The best simultaneous solution provided a reasonable synthesis of the B-band light curve (Figure 4), but less than acceptable in V- (Figure 5) and I_c-bands (Figure 6) due to marginal fits around Min I and Min II.

Significant improvement in the synthetic fit for all filters was ultimately achieved but this required modification of many modeling parameters. When setting up W-type W UMa eclipsing binaries for Roche modeling according to the Wilson-Devinney code, the reader should be aware of different approaches that appear in the literature regarding the assignment of effective temperatures for $Teff_1$ and $Teff_2$ as well as the calculations for mass ratio (q). By convention, the primary star in an eclipsing binary system is the one being eclipsed that produces the deeper minimum. In most cases but not all it is the most massive and therefore the brightest and hottest as might be predicted from luminosity-mass relationship established in Hertzsprung-Russell type diagrams. The primary star in an A-type W UMa eclipsing variable is more massive, hotter, and therefore brighter than its secondary companion. As would be expected, in this case $Teff_1$ is assigned to the primary and $Teff_2$ to the secondary, while the mass ratio (q) corresponds to m_2/m_1, a value that is less than one. It follows that the deepest minimum (Min I) or dimmest photometric reading on an A-type light curve occurs when the secondary star either transits or partially

eclipses the brighter primary star. By contrast, the effective temperature of the more massive star in a W-type W UMa binary system is somewhat cooler than its less massive stellar cohort. In this case the deepest minimum (Min I) or dimmest photometric reading on a W-type light curve occurs when the primary star either occults or partially eclipses the hotter secondary star. Under these circumstances, in order to properly execute the Wilson-Devinney code during Roche lobe modeling, an adjustment from standard convention can be made using one of two different approaches. For example, in the paper by Lee *et al.* (2009), the authors chose to define the mass ratio (q) as m_1/m_2, which in this case is 2.6897, or the reciprocal of q_{sp} (0.372), which was based upon initial radial velocity experiments by Samec and Hube (1991). This approach also requires re-defining the primary star as the hottest ($Teff_1$), rather than the most massive, and the secondary star as the coolest ($Teff_2$). The equivalent strategy taken herein, maintains the convention whereby the primary is still defined as the most massive (m_1) star, however, in this case $Teff_1 < Teff_2$ and model fitting starts by shifting the phase of the folded light curve data by 0.5. This approach where $q < 1$ is also employed by Samec and Hube (1991) and mathematically leads to a different value for the dimensionless Roche potential ($\Omega_1 = \Omega_2$) which defines the common envelope in overcontact binary systems.

Given other differences (for example, R vs. I_c filters) from the dataset produced by Lee *et al.* (2009), modeling the 2008 light curves (B, V, and I_c) collected at UO essentially started with a clean slate except for the spectroscopically determined mass ratio ($q_{sp} = 0.372$) reported by Samec and Hube (1991) and the orbital inclination ($i \approx 88°$) which is fairly consistent across all BX Peg publications. The putative effective temperature ($Teff_1$ = 5520 K) of the cooler star was based on the G7-G8V spectral classification proposed herein. BM3 requires normalized flux that has been phased; this was accomplished by MPO CANOPUS, which has a feature to prepare light curve data for BM3. Bolometric albedo ($A_{1,2} = 0.5$) and gravity darkening coefficients ($g_{1,2} = 0.32$) for cooler stars with convective envelopes were assigned according to Rucinski (1969) and Lucy (1967), respectively. Following any Teff change to either star, new logarithmic limb darkening coefficients (x_1, x_2, y_1, y_2) were interpolated according to van Hamme (1993). Values for $Teff_1$ (5520 K) and the spectroscopic mass ratio (0.372) were initially held constant while iteratively adjusting the effective temperature of the secondary ($Teff_2$), inclination (*i*), and common envelope surface potential ($\Omega_1 = \Omega_2$) until an acceptable fit of the model in a single bandpass (V) was initially obtained.

Not unexpectedly, the first iterations leading to an unspotted solution clearly indicated a marginal synthetic fit, especially during quadrature where the O'Connell effect is largely observed. To rectify this shortcoming, a cool spot on the more massive star was introduced into the model. Thereafter, model fitting with PHOEBE employed phased data that had been transformed into catalogue-based magnitudes. A_1, A_2, g_1, g_2, and $Teff_1$ were fixed parameters whereas initial

values for Ω_1 (2.60), i (88°), and $Teff_2$ (5800 K) from BM3 along with passband specific luminosity, phase shift, x_1, x_2, y_1, and y_2 were iteratively adjusted using differential corrections (DC) to achieve a simultaneous minimum residual fit of all (B, V, and I_c) photometric observations. Although Lee *et al.* (2004) had proposed the potential presence of additional mass around BX Peg based upon sinusoidal-like behavior of residuals in the ET diagram, invoking third light (l_3) in each bandpass during DC did not meaningfully improve the fit. A number of different spot solutions were attempted, most notably some which invoked the presence of an additional cool or hot spot on one or both stars. These solutions offered some improvement in the overall fits, however, they exemplify the slippery slope of trying to fit light curve data by the addition of multiple starspots. The additional degrees of freedom to the model allowed by multiple spots limits the possibility that a unique fit can be found. This was notably obvious by the increased number of iterations required to reach convergence and by the much broader error estimates for Ω_1, i, $Teff_2$, and q obtained from heuristic scanning (Prša and Zwitter 2005).

Sticking with the simplest model, the final proposed location of a single cool spot which accounts for most of the asymmetry is shown in a spatial representation for BX Peg (Figure 7). Associated unspotted and spotted light curve fits from the present study (2008) are reproduced in Figures 8 (B mag.), 9 (V mag.), and 10 (I_c mag.) while a comparison of light curve parameters and geometric elements obtained from Lee *et al.* (2009) and those collected at UO are summarized in Table 8. Importantly, excellent agreement between the spectroscopically determined (Samec and Hube 1991) mass ratio (q_{sp} = 0.372 ± 0.002) and the photometrically derived value (q_{ph} = 0.370 ± 0.005) was obtained in the present study. This is not unexpected in cases where the high orbital inclination of a contact binary leads to a total eclipse (Terrell and Wilson 2005).

3.5.2. 2011 light curves

As had been previously mentioned, in contrast to 2008 the light curves from 2011 exhibited a positive O'Connell effect where Max I was brighter than Max II. Roche model fitting with BM3 and PHOEBE was attempted using the same geometric and physical parameters derived from the 2008 light curves collected at UO, but initially without any spots. Incorporation of a single cool spot on the primary (Figure 11) facing the observer during primary minimum ultimately provided the best model fit in each filter (Figures 12–14). A comparison between light curve parameters and geometric elements obtained from Roche modeling the 2008 and 2011 light curves collected at UO is summarized in Table 6. Based upon a compilation of absolute dimensions of eclipsing binaries (Harmanec 1988), the mean stellar mass for an G7-G8 main sequence binary star (0.96 $M_\odot$) was used to derive M_1, M_2, R_1, R_2, and the semi-major axis (a) in solar units. These values (Table 7) compare favorably with those published by Samec and Hube (1991).

4. Conclusions

CCD-based photometric data collected in B, V, and I_c produced nineteen new times of minimum for BX Peg. The linear ephemeris for BX Peg was updated and potential changes in orbital periodicity were assessed through the use of ET diagrams. The ET diagram for BX Peg exhibited complex behaviors often attributed to mass transfer, magnetically active cycles, and/or the presence of an unseen mass influencing the times of minimum. However, no convincing single explanation for these periodic changes can be derived from the data extant. Different spotted solutions were necessary to achieve the best Roche model fits for BX Peg light curves collected in 2008 and 2011. Public access to any light curve data associated with this research can be obtained by request (mail@underoakobservatory.com)

5. Acknowledgements

This research has made use of the SIMBAD database, operated at Centre de Données astronomiques de Strasbourg, France. Time of minima data from the B.R.N.O., IBVS, AASVO, BAV, BBSAG, BAA VSS, and VSOLJ websites proved invaluable to the assessment of period changes experienced by this variable star. The diligence and dedication shown by all associated with these organizations is very much appreciated. I would also like to thank Professor Dirk Terrell and an unknown referee for reviewing this study report and suggesting changes which significantly improved the quality of this manuscript.

References

Agerer, F., and Hübscher, J. 2002, *Inf. Bull. Var. Stars*, No. 5296, 1.

Agerer, F., and Hübscher, J. 2003, *Inf. Bull. Var. Stars*, No. 5484, 1.

Alton, K. B. 2013, *J. Amer. Assoc. Var. Star Obs.*, **41**, in press.

Baldinelli, L., and Maitan, A. 2002, *Inf. Bull. Var. Stars*, No. 5220, 1.

Baldwin, M., and Samolyk, G. 1995, *Observed Minima Timings of Eclipsing Binaries: Number 2*, AAVSO, Cambridge, MA.

Baldwin, M., and Samolyk, G. 2004, *Observed Minima Timings of Eclipsing Binaries: Number 9*, AAVSO, Cambridge, MA.

Baldwin, M., and Samolyk, G. 2007, *Observed Minima Timings of Eclipsing Binaries: Number 12*, AAVSO, Cambridge, MA.

Beob. der Schweizerischen Astron. Ges. (BBSAG). 1987, *BBSAG Bull.*, No. 83, 1.

Beob. der Schweizerischen Astron. Ges. (BBSAG). 1988a, *BBSAG Bull.*, No. 86, 1.

Beob. der Schweizerischen Astron. Ges. (BBSAG). 1988b, *BBSAG Bull.*, No. 89, 1.

Beob. der Schweizerischen Astron. Ges. (BBSAG). 1989a, *BBSAG Bull.*, No. 90, 1.

Beob. der Schweizerischen Astron. Ges. (BBSAG). 1989b, *BBSAG Bull.*, No. 92, 1.

Beob. der Schweizerischen Astron. Ges. (BBSAG). 1990a, *BBSAG Bull.*, No. 93, 1.

Beob. der Schweizerischen Astron. Ges. (BBSAG). 1990b, *BBSAG Bull.*, No. 96, 1.
Beob. der Schweizerischen Astron. Ges. (BBSAG). 1991, *BBSAG Bull.*, No. 98, 1.
Beob. der Schweizerischen Astron. Ges. (BBSAG). 1992a, *BBSAG Bull.*, No. 99, 1.
Beob. der Schweizerischen Astron. Ges. (BBSAG). 1992b, *BBSAG Bull.*, No. 102, 1.
Beob. der Schweizerischen Astron. Ges. (BBSAG). 1994a, *BBSAG Bull.*, No. 105, 1.
Beob. der Schweizerischen Astron. Ges. (BBSAG). 1994b, *BBSAG Bull.*, No. 107, 1.
Beob. der Schweizerischen Astron. Ges. (BBSAG). 1995, *BBSAG Bull.*, No. 109, 1.
Beob. der Schweizerischen Astron. Ges. (BBSAG). 2001, *BBSAG Bull.*, No. 126, 1.
Beob. der Schweizerischen Astron. Ges. (BBSAG). 2002, *BBSAG Bull.*, No. 127, 1.
Bíró, I. B., *et al.* 2006, *Inf. Bull. Var. Stars*, No. 5684, 1.
Bradstreet, D. H., and Steelman D. P. 2002, *Bull. Amer. Astron. Soc.*, **34**, 1224.
Brát, L., Zejda, M., and Svoboda, P. 2007, *Open Eur. J. Var. Stars*, **74**, 1 (*B.R.N.O. Contrib.*, No. 34).
Brát, L., *et al.* 2011, *Open Eur. J. Var. Stars*, **137**, 1 (*B.R.N.O. Contrib.*, No. 37).
CBA Belgium Observatory. 2011, Flanders, Belgium (http://www.cbabelgium.com/).
De Young, J.A., Schmidt, R.E., and Gritz, L.I. 1991, *Inf. Bull. Var. Stars*, No. 3578.
Diethelm, R. 2003, *Inf. Bull. Var. Stars*, No. 5438, 1.
Diethelm, R. 2004, *Inf. Bull. Var. Stars*, No. 5543, 1.
Diethelm, R. 2005, *Inf. Bull. Var. Stars*, No. 5653, 1.
Diethelm, R. 2010, *Inf. Bull. Var. Stars*, No. 5920, 1.
Diethelm, R. 2011, *Inf. Bull. Var. Stars*, No. 5960, 1.
Diethelm, R. 2012, *Inf. Bull. Var. Stars*, No. 6011, 1.
Diethelm, R., Isles, J., and Locher, K. 1972, *Orion*, **30**, 60.
Doğru, S. S., Dönmez, A., Tüysüz, M., Doğru, D., Ozkardes, B., Soydugan, E., and Soydugan, F. 2007, *Inf. Bull. Var. Stars*, No. 5746, 1.
Flower, P. J. 1996, *Astrophys. J.*, **469**, 355.
Gürol, B., Gürdemir, L., Çaglar, A., Kirca, M., Akcay, U., Tunc, A., and Elmas, T. 2003, *Inf. Bull. Var. Stars*, No. 5443, 1.
Harmanec, P. 1988, *Bull. Astron. Inst. Czechoslovakia*, **39**, 329.
Hoffmann, M. 1982, *Acta Astron.*, **32**, 131.
Hübscher, J. 2005, *Inf. Bull. Var. Stars*, No. 5643, 1.
Hübscher, J. 2011, *Inf. Bull. Var. Stars*, No. 5984, 1.
Hübscher, J., Agerer F., Frank, P., and Wunder, E. 1994, *BAV Mitt.*, No. 68, 1.
Hübscher, J., Agerer F., and Wunder, E. 1992, *BAV Mitt.*, No. 60, 1.
Hübscher, J., Agerer F., and Wunder, E. 1993, *BAV Mitt.*, No. 62, 1 .
Hübscher, J., and Lichtenknecker, D. 1988, *BAV Mitt.*, No. 50, 1.
Hübscher, J., Lichtenknecker, D., and Meyer, J. 1986, *BAV Mitt.*, No. 43, 1.
Hübscher, J., Lichtenknecker, D., and Wunder, E. 1989, *BAV Mitt.*, No. 52, 1.
Hübscher, J., Lichtenknecker, D., and Wunder, E. 1990, *BAV Mitt.*, No. 56, 1.
Hübscher, J., and Mundry, E. 1984, *BAV Mitt.*, No. 38, 1.
Hübscher, J., Paschke, A., and Walter, F. 2005, *Inf. Bull. Var. Stars*, No. 5657, 1.

Hübscher, J., Paschke, A., and Walter, F. 2006, *Inf. Bull. Var. Stars*, No. 5731, 1.
Hübscher, J., Steinbach, H-M., and Walter, F. 2009, *Inf. Bull. Var. Stars*, No. 5889, 1.
Hübscher, J., and Walter, F. 2007, *Inf. Bull. Var. Stars*, No. 5761, 1.
Isles, J. 1985a, *Br. Astron. Assoc. Var. Star Sect. Circular*, No. 59, 14.
Isles, J. 1985b, *Br. Astron. Assoc. Var. Star Sect. Circular*, No. 60, 15.
Isles, J. 1985c, *Br. Astron. Assoc. Var. Star Sect. Circular*, No. 61, 14.
Isles, J. 1989, *Br. Astron. Assoc. Var. Star Sect. Circular*, No. 68, 30.
Isles, J. 1992, *Br. Astron. Assoc. Var. Star Sect. Circular*, No. 73, 13.
Kaluzny, J. 1984, *Acta Astron.*, **34**, 217.
Krajci, T. 2005, *Inf. Bull. Var. Stars*, No. 5592, 1.
Kreiner, J. M. 2004, *Acta Astron.*, **54**, 207.
Kwee, K. K., and van Woerden, H. 1956, *Bull. Astron. Inst. Netherlands*, **12**, 327.
Lee, J. W., Kim, C-H., Han, W., Kim, H-I., and Koch, R. H. 2004, *Mon. Not. Roy. Astron. Soc.*, **352**, 1041.
Lee, J. W., Kim, S-L., Lee, C-U., and Youn, J-H. 2009, *Publ. Astron. Soc. Pacific*, **886**, 1366.
Leung, K-C., Zhai, D., and Zhang, Y. 1985, *Astron. J.*, **90**, 515.
Lucy, L. B. 1967, *Z. Astrophys.*, **65**, 89.
Maceroni, C., and van't Veer, F. 1996, *Astron. Astrophys.*, **311**, 523.
Maciejewski, G., and Karska, A. 2004, *Inf. Bull. Var. Stars*, No. 5494.
Mikulášek, Z. (ed.). 1985, *Contrib. Nicholas Copernicus Obs. Planetarium Brno*, No. 26, 5.
Mikulášek, Z. (ed.). 1986, *Contrib. Nicholas Copernicus Obs. Planetarium Brno*, No. 27, 5.
Mikulášek, Z., and Šilhán, J. (eds.). 1988, *Contrib. Nicholas Copernicus Obs. Planetarium Brno*, No. 28, 6.
Mikulášek, Z., Šilhán, J., and Zejda, M. (eds.). 1992, *Contrib. Nicholas Copernicus Obs. Planetarium Brno*, No. 30, 4.
Mikulášek, Z., and Zejda, M. (eds.) 2002, *Contrib. Nicholas Copernicus Obs. Planetarium Brno*, No. 32, 5.
Minor Planet Observer. 2010, MPO Software Suite (http://www.minorplanetobserver.com), BDW Publishing, Colorado Springs.
Nagai, K. 2003, *VSOLJ Var. Star Bull.*, No. 40, 1.
Nagai, K. 2006, *VSOLJ Var. Star Bull.*, No. 44, 1.
Nagai, K. 2007, *VSOLJ Var. Star Bull.*, No. 45, 1.
Nagai, K. 2008, *VSOLJ Var. Star Bull.*, No. 46, 1.
Nagai, K. 2010, *VSOLJ Var. Star Bull.*, No. 50, 1.
Nagai, K. 2012, *VSOLJ Var. Star Bull.*, No. 53, 1.
Nelson, R. H. 2001, *Inf. Bull. Var. Stars*, No. 5040, 1.
Nelson, R. H. 2002, *Inf. Bull. Var. Stars*, No. 5224, 1.
Nelson, R. H. 2003, *Inf. Bull. Var. Stars*, No. 5371, 1.

Nelson, R. H. 2007, Minima©2002–2006: Astronomy Software by Bob Nelson (http://members.shaw.ca/bob.nelson/software1.htm).
Nelson, R. H. 2009, WDwint56a: Astronomy Software by Bob Nelson (http://members.shaw.ca/bob.nelson/software1.htm).
Ogloza, W., Niewiadomski, W., Barnacka, A., Biskup, M., Malek, K., and Sokolowski, M. 2008, *Inf. Bull. Var. Stars*, No. 5843, 1.
Parimucha, Š., Dubovský, P., Baludanský, D., Pribulla, T., Hambalek, L., Vanko, M., and Ogloza, W. 2009, *Inf. Bull. Var. Stars*, No. 5898, 1.
Parimucha, Š., Dubovský, P., Vanko, M., Pribulla, T., Kudzej, I., and Barsa, R. 2011, *Inf. Bull. Var. Stars*, No. 5980, 1.
Paschke, A. 2007, *Open Eur. J. Var. Stars*, **73**, 1.
Pribulla, T., *et al.* 2005, *Inf. Bull. Var. Stars*, No. 5668, 1.
Prša, A., and Harmanec, P. 2010, *PHOEBE Manual, Adopted for PHOEBE 0.32*, Villanova Univ., Radnor Township, PA.
Prša, A., and Zwitter, T. 2005, *Astrophys. J.*, **628**, 426.
Ruciński, S. M. 1969, *Acta Astron.*, **19**, 245.
Šafář, J., and Zejda, M. 2000a, *Inf. Bull. Var. Stars*, No. 4887, 1.
Šafář, J., and Zejda, M. 2000b, *Inf. Bull. Var. Stars*, No. 4888, 1.
Samec, R. G. 1989, *Inf. Bull. Var. Stars*, No. 3392, 1.
Samec, R. G. 1990, *Astron. J.*, **100**, 808.
Samec, R. G., and Bookmyer, B. B. 1987, *Inf. Bull. Var. Stars*, No. 2999, 1.
Samec, R. G., and Hube, D. P. 1991, *Astron. J.*, **102**, 1171.
Samolyk, G. 2008a, *J. Amer. Assoc. Var. Star Obs.*, **36**, 171.
Samolyk, G. 2008b, *J. Amer. Assoc. Var. Star Obs.*, **36**, 186.
Samolyk, G. 2009, *J. Amer. Assoc. Var. Star Obs.*, **37**, 44.
Samolyk, G. 2010, *J. Amer. Assoc. Var. Star Obs.*, **38**, 183.
Schwarzenberg-Czerny, A. 1996, *Astrophys. J., Lett.*, **460**, L107.
Shapley, H., and Hughes, E. M. 1934, *Ann. Harvard Coll. Obs.*, **90**, 163.
Terrell, D., and Wilson, R. E. 2005, *Astrophys. Space Sci.*, **296**, 221.
van Hamme, W. 1993, *Astron. J.*, **106**, 2096.
Warner, B. 2007, *Minor Planet Bull.*, **34**, 113.
Wilson, R. E. 1979, *Astrophys. J.*, **234**, 1054.
Wilson, R. E., and Devinney, E. J. 1971, *Astrophys. J.*, **166**, 605.
Yakut, K., and Eggleton, P. P. 2005, *Astrophys. J.*, **629**, 1055.
Zejda, M. (ed.). 1995, *Contrib. Nicholas Copernicus Obs. Planetarium Brno*, 31, 4.
Zejda, M. 2004, *Inf. Bull. Var. Stars*, No. 5583, 1.
Zejda, M., Mikulásek, Z., and Wolf, M. 2006, *Inf. Bull. Var. Stars*, No. 5741, 1.
Zhai, D-S., and Zhang, R-X. 1979, *Kexue Tongbao*, **24**, 986.

Table 1. Astrometric coordinates (J2000) and MPOSC3 catalogue magnitudes (V, B, and I_c) for BX Peg and five comparison stars used in this photometric study.

Star Identification	*R.A.* h m s	*Dec.* ° ′ ″	*MPOSC3*[a] *B mag.*	*MPOSC3 V mag.*	*MPOSC3 I_c mag.*	*MPOSC3 (B–V)*
BX Peg	21 38 49.39	26 41 34.2	11.54–12.29[b]	10.8–11.53	10.0–10.63	0.812
C1	21 38 57.74	26 36 51.4	13.154	12.694	12.145	0.460
C2	21 39 00.59	26 38 10.4	13.327 (13.51)[c]	12.678 (12.77)[c]	11.95	0.649
C3	21 39 02.87	26 38 43.0	13.384 (13.37)[c]	12.287 (12.34)[c]	11.16 (11.20)[c]	1.097
C4	21 39 07.72	26 44 37.4	13.219	12.736	12.164	0.483
C5	21 39 00.86	26 44 58.8	13.88	13.044	12.151	0.836

Notes: *a. MPOSC3 (Warner 2007) is a hybrid catalogue which includes a large subset of the Carlsberg Meridian Catalog (CMC–14) as well as data from the Sloan Digital Sky Survey (SDSS). b. Range of magnitudes in light curves for each variable. c. AAVSO comparison star magnitudes in parentheses.*

Table 2. New times of minimum for BX Peg acquired at UnderOak Observatory.

Mean Computed Time of Minimum (HJD–2400000)[a]	*Error ±*	*UT Date of Observations*	*Type of Minimum*[a]
54747.5240	0.0009	08 Oct 2008	p
54751.5902	0.0006	12 Oct 2008	s
54752.5717	0.0006	13 Oct 2008	p
54755.5162	0.0008	16 Oct 2008	s
54759.5823	0.0004	20 Oct 2008	p
54763.5074	0.0004	24 Oct 2008	p
54766.5924	0.0004	27 Oct 2008	p
54770.5181	0.0008	31 Oct 2008	p
55840.5864	0.0006	06 Oct 2011	p
55841.5688	0.0005	07 Oct 2011	s
55841.7066	0.0009	07 Oct 2011	p
55842.5496	0.0006	08 Oct 2011	p
55842.6906	0.0008	08 Oct 2011	s
55843.5316	0.0007	09 Oct 2011	s
55843.6709	0.0005	09 Oct 2011	p
55844.6535	0.0008	10 Oct 2011	s
55868.4890	0.0007	02 Nov 2011	s
55868.6282	0.0008	03 Nov 2011	p
55873.5372	0.0005	08 Nov 2011	s

Note: a. s = secondary; p = primary

Table 3. Visual, Photographic, Photoelectric, and CCD Times of Minimum (–2,400,000) for BX Peg from 1960 to 2011. Eclipse timing residuals $(ETR)_1$ are based on the linear elements defined by Kreiner (2004).

Time of Minimum	*Cycle Mumber*	*Source*	$(ETR)_1$	*Ref.**	*Time of Minimum*	*Cycle Mumber*	*Source*	$(ETR)_1$	*Ref.**
37225.6274	–54470.5	PE	–0.136572	1	44195.2373	–29616.5	PE	–0.028188	5
41249.276	–40122	vis	–0.061341	2	44195.3771	–29616	PE	–0.028597	5
43042.715	–33726.5	vis	–0.033741	3	44474.825	–28619.5	vis	–0.016935	3
43079.725	–33594.5	vis	–0.038877	3	44539.601	–28388.5	vis	–0.017424	3
43096.557	–33534.5	vis	–0.031939	3	44544.653	–28370.5	vis	–0.012942	3
43380.755	–32521	vis	–0.037278	3	44822.403	–27380	vis	–0.016674	6
43452.688	–32264.5	vis	–0.031418	3	44843.423	–27305	vis	–0.028001	7
43452.691	–32264.5	vis	–0.028418	3	44843.574	–27304.5	vis	–0.017210	7
43714.739	–31330	vis	–0.030759	3	44844.409	–27301.5	vis	–0.023463	7
43757.644	–31177	vis	–0.029667	3	44869.375	–27212.5	vis	–0.014639	7
43790.0303	–31061.5	PE	–0.031611	1	44880.730	–27172	vis	–0.016556	3
43790.1704	–31061	PE	–0.031720	1	44926.577	–27008.5	vis	–0.017850	3
43790.1708	–31061	PE	–0.031320	4	45175.460	–26121	vis	–0.005558	8
43791.0126	–31058	PE	–0.030773	1	45191.430	–26064	vis	–0.019367	8
43791.1524	–31057.5	PE	–0.031182	1	45195.500	–26049.5	vis	–0.015424	8
43802.650	–31016.5	vis	–0.030708	3	45197.456	–26042.5	vis	–0.022348	8
43840.0847	–30883	PE	–0.031771	1	45291.687	–25706.5	vis	–0.011695	3
43844.9908	–30865.5	PE	–0.032981	1	45561.446	–24744.5	vis	–0.014522	8
44101.724	–29950	vis	–0.022185	3	45566.487	–24726.5	vis	–0.021041	8
44128.648	–29854	vis	–0.018284	3	45573.374	–24702	vis	–0.004275	8

Table continued on following pages

Table 3. Visual, Photographic, Photoelectric, and CCD Times of Minimum (–2,400,000) for BX Peg from 1960 to 2011. Eclipse timing residuals $(ETR)_1$ are based on the linear elements defined by Kreiner (2004).

Time of Minimum	*Cycle Mumber*	*Source*	*$(ETR)_1$*	*Ref.**	*Time of Minimum*	*Cycle Mumber*	*Source*	*$(ETR)_1$*	*Ref.**
45576.451	–24691	vis	–0.011869	8	46028.626	–23078.5	vis	–0.010411	3
45577.443	–24687.5	vis	–0.001331	8	46028.636	–23078.5	vis	–0.000411	3
45605.335	–24588	vis	–0.010892	9	46271.4864	–22212.5	vis	0.008261	11
45605.476	–24587.5	vis	–0.010101	9	46289.4426	–22148.5	vis	0.017728	11
45621.317	–24531	vis	–0.012701	9	46292.5148	–22137.5	vis	0.005334	11
45621.458	–24530.5	vis	–0.011910	9	46292.5231	–22137.5	vis	0.013634	11
45640.2445	–24463.5	PE	–0.013396	9	46292.5252	–22137.5	vis	0.015734	11
45646.2746	–24442	PE	–0.012277	9	46292.5273	–22137.5	vis	0.017834	11
45651.3219	–24424	PE	–0.012495	9	46292.5273	–22137.5	vis	0.017834	11
45701.649	–24244.5	vis	–0.020372	3	46292.5273	–22137.5	vis	0.017834	11
45925.444	–23446.5	vis	0.001303	10	46292.5280	–22137.5	vis	0.018534	11
45932.441	–23421.5	vis	–0.012139	10	46292.5280	–22137.5	vis	0.018534	11
45933.428	–23418	vis	–0.006601	10	46293.6380	–22133.5	vis	0.006863	3
45942.407	–23386	vis	–0.000968	10	46297.414	–22120	vis	–0.002776	12
45945.769	–23374	vis	–0.003980	3	46318.311	–22045.5	vis	0.003105	13
45956.710	–23335	vis	0.000729	3	46319.422	–22041.5	pg	–0.007565	13
45959.655	–23324.5	vis	0.001344	3	46327.284	–22013.5	vis	0.002739	13
45962.591	–23314	vis	–0.007042	3	46351.400	–21927.5	vis	0.002817	12
45964.593	–23307	vis	0.032034	3	46352.286	–21924.5	vis	0.047564	12
45975.530	–23268	vis	0.032744	3	46380.278	–21824.5	vis	–0.002206	12

Table continued on following pages

Table 3. Visual, Photographic, Photoelectric, and CCD Times of Minimum (–2,400,000) for BX Peg from 1960 to 2011. Eclipse timing residuals $(ETR)_1$ are based on the linear elements defined by Kreiner (2004).

Time of Minimum	*Cycle Mumber*	*Source*	$(ETR)_1$	*Ref.**	*Time of Minimum*	*Cycle Mumber*	*Source*	$(ETR)_1$	*Ref.**
46612.4885	–20996.5	vis	0.022438	14	46728.284	–20583.5	vis	0.005428	14
46612.4899	–20996.5	vis	0.023838	14	46743.283	–20530	vis	0.002081	15
46619.4786	–20971.5	vis	0.002096	14	47039.548	–19473.5	pg	0.005781	16
46619.4793	–20971.5	vis	0.002796	14	47055.390	–19417	vis	0.004181	17
46619.4807	–20971.5	vis	0.004196	14	47056.360	–19413.5	vis	–0.007281	17
46641.487	–20893	vis	–0.002294	12	47057.348	–19410	vis	–0.000743	17
46659.435	–20829	vis	–0.001027	12	47333.8400	–18424	PE	–0.000595	4
46667.423	–20800.5	vis	–0.004931	12	47362.452	–18322	vis	0.008799	18
46678.3706	–20761.5	vis	0.006379	14	47374.360	–18279.5	vis	–0.000953	18
46678.3768	–20761.5	vis	0.012579	14	47378.432	–18265	vis	0.004990	18
46678.3831	–20761.5	vis	0.018879	14	47381.395	–18254.5	vis	0.023605	18
46678.5247	–20761	vis	0.020270	14	47387.5412	–18232.5	vis	0.000615	19
46678.5261	–20761	vis	0.021670	14	47389.5140	–18225.5	vis	0.010491	18
46678.5268	–20761	vis	0.022370	14	47405.491	–18168.5	pg	0.003682	20
46688.4580	–20725.5	vis	–0.001259	12	47450.6339	–18007.5	PE	–0.000667	1
46701.7787	–20678	PE	–0.000399	5	47451.7556	–18003.5	PE	–0.000638	1
46703.7409	–20671	PE	–0.001123	5	47469.293	–17941	vis	0.010656	3
46703.8797	–20670.5	PE	–0.002532	5	47524.242	–17745	vis	–0.002214	21
46704.7227	–20667.5	PE	–0.000785	5	47727.408	–17020.5	pg	0.001163	22
46709.640	–20650	vis	0.009205	3	47727.548	–17020	pg	0.000954	22

Table continued on following pages

Table 3. Visual, Photographic, Photoelectric, and CCD Times of Minimum (–2,400,000) for BX Peg from 1960 to 2011. Eclipse timing residuals $(ETR)_1$ are based on the linear elements defined by Kreiner (2004).

Time of Minimum	*Cycle Mumber*	*Source*	*$(ETR)_1$*	*Ref.**	*Time of Minimum*	*Cycle Mumber*	*Source*	*$(ETR)_1$*	*Ref.**
47734.448	–16995.5	vis	0.030720	19	48120.4212	–15619	vis	0.008956	26
47734.448	–16995.5	vis	0.030720	19	48120.4233	–15619	vis	0.011056	26
47742.442	–16967	vis	0.032816	23	48120.4302	–15619	vis	0.017956	26
47757.408	–16913.5	vis	–0.003531	24	48120.4316	–15619	vis	0.019356	26
47762.456	–16895.5	vis	–0.003050	24	48120.4323	–15619	vis	0.020056	26
47790.358	–16796	pg	–0.002611	22	48121.419	–15615.5	vis	0.025294	27
47813.354	–16714	vis	–0.000862	24	48126.459	–15597.5	vis	0.017776	27
47817.300	–16700	vis	0.019290	25	48147.330	–15523	vis	–0.002343	27
47822.327	–16682	pg	–0.001229	22	48174.274	–15427	vis	0.021558	27
47822.3275	–16682	PE	–0.000729	22	48174.5303	–15426	CCD	–0.002560	28
47822.3278	–16682	PE	–0.000429	22	48187.285	–15380.5	vis	–0.006865	27
47838.3310	–16625	vis	0.018962	25	48189.384	–15373	vis	–0.010998	27
47847.2843	–16593	PE	–0.001004	22	48191.4989	–15365.5	CCD	0.000769	28
47847.2844	–16593	PE	–0.001004	22	48213.5094	–15287	CCD	–0.001520	28
47847.2850	–16593	vis	–0.000404	24	48225.5672	–15244	CCD	–0.001681	28
47854.299	–16568	vis	0.003154	25	48225.5681	–15244	CCD	–0.000781	28
47859.360	–16550	vis	0.016635	25	48419.5004	–14552.5	vis	0.022679	26
47859.633	–16549	vis	0.009217	3	48438.454	–14485	vis	0.048084	29
48085.5081	–15743.5	vis	0.007860	26	48439.403	–14481.5	vis	0.015623	29
48120.4142	–15619	vis	0.001956	26	48444.451	–14463.5	vis	0.016104	29

Table continued on following pages

Table 3. Visual, Photographic, Photoelectric, and CCD Times of Minimum (–2,400,000) for BX Peg from 1960 to 2011. Eclipse timing residuals $(ETR)_1$ are based on the linear elements defined by Kreiner (2004).

Time of Minimum	*Cycle Mumber*	*Source*	$(ETR)_1$	*Ref.**	*Time of Minimum*	*Cycle Mumber*	*Source*	$(ETR)_1$	*Ref.**
48479.376	–14339	vis	0.029100	29	49171.5549	–11870.5	PE	–0.003092	34
48491.4017	–14296	PE	–0.003161	30	49214.4502	–11717.5	vis	–0.011700	26
48491.4023	–14296	PE	–0.002561	30	49218.5212	–11703	vis	–0.006757	26
48499.540	–14267	pg	0.003026	31	49228.3394	–11668	PE	–0.003176	34
48500.402	–14264	vis	0.023773	29	49250.3510	–11589.5	CCD	–0.004366	35
48507.420	–14239	vis	0.031330	32	49250.4910	–11589	CCD	–0.004575	35
48518.360	–14200	vis	0.035040	32	49317.2317	–11351	PE	–0.003287	34
48828.458	–13094	vis	–0.008936	26	49568.394	–10455.5	vis	0.044962	36
48834.4922	–13072.5	vis	–0.003717	26	49624.586	–10255	vis	0.013214	3
48834.4971	–13072.5	vis	0.001183	26	49897.459	–9282	vis	0.039791	37
48834.4984	–13072.5	vis	0.002483	26	49920.555	–9199.5	vis	0.001331	38
48837.480	–13062	vis	0.039697	33	49923.4918	–9189	vis	–0.006255	38
48862.418	–12973	vis	0.020522	33	50282.4339	–7909	vis	0.001189	38
48882.359	–12902	vis	0.051865	33	50282.4346	–7909	vis	0.001889	38
48883.338	–12898.5	vis	0.049403	33	50282.4373	–7909	vis	0.004589	38
48914.585	–12787	vis	0.029830	3	50282.4394	–7909	vis	0.006689	38
48922.565	–12758.5	vis	0.017925	3	50282.4429	–7909	vis	0.010189	38
48946.275	–12674	vis	0.032630	33	50316.3607	–7788	CCD	–0.002552	39
48954.529	–12644.5	vis	0.014308	3	50316.5003	–7787.5	CCD	–0.003161	39
49171.4142	–11871	PE	–0.003583	34	50376.671	–7573	vis	0.017942	40

Table continued on following pages

Table 3. Visual, Photographic, Photoelectric, and CCD Times of Minimum (–2,400,000) for BX Peg from 1960 to 2011. Eclipse timing residuals $(ETR)_1$ are based on the linear elements defined by Kreiner (2004).

Time of Minimum	*Cycle Mumber*	*Source*	*$(ETR)_1$*	*Ref.**	*Time of Minimum*	*Cycle Mumber*	*Source*	*$(ETR)_1$*	*Ref.**
50703.4593	–6407.5	vis	–0.020587	38	51434.5232	–3800.5	vis	–0.005631	38
50707.5502	–6393	CCD	0.004256	39	51470.0005	–3674	CCD	–0.001170	42
50713.2946	–6372.5	CCD	0.000093	39	51470.1399	–3673.5	CCD	–0.001979	42
50726.648	–6325	vis	0.033653	40	51477.0109	–3649	CCD	–0.001213	42
50829.2453	–5959	CCD	–0.001926	41	51477.1507	–3648.5	CCD	–0.001622	42
50990.4783	–5384	vis	–0.009103	38	51500.9856	–3563.5	CCD	–0.002226	42
51021.4704	–5273.5	vis	–0.003159	38	51758.4227	–2645.5	vis	0.011425	43
51021.4725	–5273.5	vis	–0.001059	38	51758.4234	–2645.5	vis	0.012125	43
51021.4753	–5273.5	vis	0.001741	38	51758.4269	–2645.5	vis	0.015625	43
51031.4291	–5238	vis	0.000713	38	51758.4317	–2645.5	vis	0.020425	43
51032.409	–5234.5	vis	–0.000849	38	51758.4352	–2645.5	vis	0.023925	43
51084.588	–5048.5	vis	0.020458	40	51761.9155	–2633	CCD	–0.001046	44
51156.505	–4792	vis	0.010318	40	51791.0798	–2529	CCD	–0.000137	42
51432.4232	–3808	vis	–0.002498	38	51791.2196	–2528.5	CCD	–0.000546	42
51432.4253	–3808	vis	–0.000398	38	51837.636	–2363	vis	0.006725	40
51432.4309	–3808	vis	0.005202	38	51899.3225	–2143	CCD	0.001331	43
51433.4059	–3804.5	vis	–0.001260	38	52015.9750	–1727	CCD	0.000068	45
51433.408	–3804.5	vis	0.000840	38	52121.4173	–1351	CCD	0.005313	46
51433.4128	–3804.5	vis	0.005640	38	52121.4212	–1351	CCD	0.009213	47
51433.4163	–3804.5	vis	0.009140	38	52133.766	–1307	vis	0.015634	40

Table continued on following pages

Table 3. Visual, Photographic, Photoelectric, and CCD Times of Minimum (–2,400,000) for BX Peg from 1960 to 2011. Eclipse timing residuals $(ETR)_1$ are based on the linear elements defined by Kreiner (2004).

Time of Minimum	*Cycle Mumber*	*Source*	$(ETR)_1$	*Ref.**	*Time of Minimum*	*Cycle Mumber*	*Source*	$(ETR)_1$	*Ref.**
52137.3969	–1294	CCD	0.001104	48	52521.5697	76	CCD	0.0016548	49
52137.5365	–1293.5	CCD	0.000495	48	52546.6670	165.5	CCD	0.0016006	53
52145.5289	–1265	CCD	0.000990	49	52560.9727	216.5	CCD	0.0059679	54
52194.3215	–1091	CCD	0.000911	50	52561.1123	217	CCD	0.0053591	54
52201.6134	–1065	CCD	0.001951	40	52565.5965	233	CCD	0.0028759	40
52219.558	–1001	vis	–0.000182	40	52602.6112	365	CCD	0.0024395	40
52240.5917	–926	CCD	0.002190	40	52806.7546	1093	CCD	0.001754	40
52465.473	–124	vis	–0.011505	43	52815.4469	1124	PE	0.001065	55
52465.4744	–124	vis	–0.010115	43	52815.4500	1124	PE	0.004175	55
52478.3855	–78	CCD	0.001781	40	52870.6902	1321	CCD	0.002118	40
52496.6128	–13	CCD	0.001930	40	52878.4018	1348.5	CCD	0.002232	56
52501.3783	4	CCD	0.000329	40	52878.5425	1349	CCD	0.002723	56
52501.6256	5	CCD	–0.032789	51	52886.3935	1377	CCD	0.002027	57
52504.4752	15	vis	0.0126345	43	52887.3756	1380.5	CCD	0.002665	58
52505.4453	18.5	CCD	0.0012725	52	52887.5149	1381	CCD	0.001756	58
52505.5859	19	CCD	0.0016637	52	52887.5150	1381	CCD	0.001856	59
52510.4923	36.5	CCD	0.0007540	52	52902.3758	1434	CCD	0.000518	58
52514.6663	51.5	CCD	–0.031512	51	52908.4028	1455.5	vis	–0.001462	43
52517.5164	61.5	vis	0.0143614	43	52914.7150	1478	CCD	0.001339	60
52521.4288	75.5	CCD	0.0009637	49	52914.8564	1478.5	CCD	0.002531	60

Table continued on following pages

Table 3. Visual, Photographic, Photoelectric, and CCD Times of Minimum (–2,400,000) for BX Peg from 1960 to 2011. Eclipse timing residuals $(ETR)_1$ are based on the linear elements defined by Kreiner (2004).

Time of Minimum	*Cycle Mumber*	*Source*	*$(ETR)_1$*	*Ref.**	*Time of Minimum*	*Cycle Mumber*	*Source*	*$(ETR)_1$*	*Ref.**
52920.6030	1499	CCD	0.000568	40	53228.3612	2596.5	CCD	0.000342	43
52929.4367	1530.5	CCD	0.001110	58	53233.4095	2614.5	CCD	0.001123	56
52929.5793	1531	CCD	0.003501	58	53233.5488	2615	CCD	0.000214	56
52931.3934	1537.5	vis	–0.005074	43	53236.3538	2625	CCD	0.001037	61
52941.3539	1573	vis	0.000598	43	53236.4931	2625.5	CCD	0.000129	61
52956.3592	1626.5	CCD	0.003511	43	53240.4180	2639.5	CCD	–0.000819	61
52986.5020	1734	CCD	0.001408	40	53240.5597	2640	CCD	0.000672	61
53208.4530	2525.5	CCD	0.001799	61	53250.3747	2675	CCD	0.001052	56
53209.4332	2529	CCD	0.000537	56	53250.5084	2675.5	CCD	–0.005426	62
53209.4335	2529	CCD	0.000837	61	53250.5140	2675.5	CCD	0.000144	56
53209.5743	2529.5	CCD	0.001428	61	53252.6171	2683	CCD	0.000111	63
53212.5180	2540	CCD	0.000742	61	53255.4219	2693	CCD	0.000734	56
53217.4262	2557.5	CCD	0.001632	56	53255.5628	2693.5	CCD	0.001425	56
53220.3701	2568	CCD	0.001146	61	53257.3845	2700	CCD	0.000410	56
53220.5099	2568.5	CCD	0.000738	61	53257.5226	2700.5	CCD	–0.001699	56
53220.5112	2568.5	CCD	0.002038	56	53277.5746	2772	CCD	0.000436	63
53221.4928	2572	CCD	0.002176	56	53282.3417	2789	CCD	0.000435	56
53224.4358	2582.5	CCD	0.000790	61	53282.4834	2789.5	CCD	0.001926	56
53226.5392	2590	CCD	0.001057	56	53341.2285	2999	CCD	–0.000482	64
53226.5392	2590	CCD	0.001057	61	53360.2974	3067	CCD	0.000014	65

Table continued on following pages

Table 3. Visual, Photographic, Photoelectric, and CCD Times of Minimum (–2,400,000) for BX Peg from 1960 to 2011. Eclipse timing residuals $(ETR)_1$ are based on the linear elements defined by Kreiner (2004).

Time of Minimum	*Cycle Mumber*	*Source*	*$(ETR)_1$*	*Ref.**	*Time of Minimum*	*Cycle Mumber*	*Source*	*$(ETR)_1$*	*Ref.**
53589.6777	3885	CCD	–0.001364	63	53951.2770	5174.5	CCD	–0.000689	69
53601.4569	3927	CCD	0.000292	66	53966.4203	5228.5	CCD	0.000056	70
53613.3741	3969.5	CCD	–0.000260	66	53966.5597	5229	CCD	–0.000753	70
53613.5150	3970	CCD	0.000431	65	53985.4890	5296.5	CCD	0.000352	71
53613.5159	3970	CCD	0.001331	66	53987.9119	5305	CCD	0.039701	72
53614.3566	3973	CCD	0.000778	43	53989.6960	5311.5	CCD	0.001086	72
53614.4970	3973.5	CCD	0.000969	66	53992.3574	5321	CCD	–0.001482	70
53616.4573	3980.5	CCD	–0.001655	43	53992.3628	5321	CCD	0.003908	43
53617.4407	3984	CCD	0.000283	43	54000.3487	5349.5	CCD	–0.002086	43
53632.0216	4036	CCD	–0.000537	67	54002.4524	5357	CCD	–0.001519	70
53632.1623	4036.5	CCD	–0.000046	67	54079.5669	5632	CCD	–0.001886	63
53648.4272	4094.5	CCD	0.000627	66	54279.6470	6345.5	CCD	0.000185	73
53651.3711	4105	CCD	0.000141	43	54281.7505	6353	CCD	0.000552	63
53651.3714	4105	CCD	0.000442	66	54297.4537	6409	CCD	0.000361	68
53651.5111	4105.5	CCD	–0.000067	66	54327.4581	6516	CCD	0.000067	43
53659.3629	4133.5	CCD	0.000037	66	54328.4386	6519.5	CCD	–0.000865	43
53659.5033	4134	CCD	0.000228	66	54328.4393	6519.5	CCD	–0.000195	43
53663.9891	4150	CCD	–0.000655	67	54330.5428	6527	CCD	0.000202	43
53928.4221	5093	CCD	–0.001546	68	54330.5431	6527	CCD	0.000472	43
53951.1360	5174	CCD	–0.001480	69	54359.9874	6632	CCD	0.000914	74

Table continued on following pages

Table 3. Visual, Photographic, Photoelectric, and CCD Times of Minimum (–2,400,000) for BX Peg from 1960 to 2011. Eclipse timing residuals $(ETR)_1$ are based on the linear elements defined by Kreiner (2004).

Time of Minimum	*Cycle Mumber*	*Source*	*$(ETR)_1$*	*Ref.**	*Time of Minimum*	*Cycle Mumber*	*Source*	*$(ETR)_1$*	*Ref.**
54386.6281	6727	CCD	0.001932	75	54760.7033	8061	CCD	–0.000080	78
54393.9200	6753	CCD	0.002972	74	54761.6856	8064.5	CCD	0.000758	78
54420.5567	6848	CCD	–0.000010	75	54763.5079	8071	CCD	–0.000157	79
54650.7799	7669	CCD	0.000259	76	54766.5923	8082	CCD	0.000249	79
54678.4008	7767.5	CCD	0.000015	68	54770.5184	8096	CCD	0.000101	79
54690.4604	7810.5	CCD	0.001654	68	54785.6608	8150	CCD	0.000245	78
54702.6579	7854	CCD	0.000984	76	54786.6426	8153.5	CCD	0.000583	78
54721.7261	7922	CCD	0.000781	77	55000.4587	8916	CCD	–0.001813	81
54736.7282	7975.5	CCD	0.000534	78	55000.4587	8916	CCD	–0.001813	81
54736.8681	7976	CCD	0.000225	78	55000.4590	8916	CCD	–0.001513	81
54737.7092	7979	CCD	0.000072	78	55057.3837	9119	CCD	–0.001606	82
54737.8500	7979.5	CCD	0.000663	78	55061.0300	9132	CCD	–0.000736	83
54738.6912	7982.5	CCD	0.000610	78	55061.1705	9132.5	CCD	–0.000445	83
54747.5241	8014	CCD	0.000252	79	55082.0685	9207	CCD	0.006436	83
54751.5906	8028.5	CCD	0.000396	79	55087.6684	9227	CCD	–0.002018	84
54752.5719	8032	CCD	0.000434	79	55107.2959	9297	CCD	–0.003757	84
54755.5164	8042.5	CCD	0.000548	79	55121.6025	9348	CCD	0.001540	85
54757.3391	8049	CCD	0.000733	80	55121.7390	9348.5	CCD	–0.002168	85
54759.5824	8057	CCD	0.000591	79	55146.5572	9437	CCD	–0.000935	84
54759.7225	8057.5	CCD	0.000582	78	55383.7904	10283	CCD	–0.001109	86

Table continued on next page

Table 3. Visual, Photographic, Photoelectric, and CCD Times of Minimum (–2,400,000) for BX Peg from 1960 to 2011. Eclipse timing residuals $(ETR)_1$ are based on the linear elements defined by Kreiner (2004).

Time of Minimum	*Cycle Mumber*	*Source*	*$(ETR)_1$*	*Ref.**	*Time of Minimum*	*Cycle Mumber*	*Source*	*$(ETR)_1$*	*Ref.**
55481.3719	10631	CCD	–0.004969	87	55843.6711	11923	CCD	–0.005637	79
55481.5166	10631.5	CCD	–0.000478	87	55844.6536	11926.5	CCD	–0.004499	79
55482.3561	10634.5	CCD	–0.002231	82	55849.7021	11944.5	CCD	–0.003418	88
55840.5864	11912	CCD	–0.005542	79	55850.6809	11948	CCD	–0.006080	88
55841.5692	11915.5	CCD	–0.004604	79	55856.5550	11969	vis	–0.020751	89
55841.7065	11916	CCD	–0.007013	79	55868.4891	12011.5	CCD	–0.004504	79
55842.5498	11919	CCD	–0.005266	79	55868.6284	12012	CCD	–0.005512	79
55842.6907	11919.5	CCD	–0.004475	79	55873.5372	12029.5	CCD	–0.003822	79
55843.5318	11922.5	CCD	–0.004728	79					

** References:; (1) Samec 1990; (2) Diethelm et al. 1972; (3) Baldwin and Samolyk 1995; (4) Samec 1989; (5) Samec and Bookmyer 1987; (6) Mikulášek 1985; (7) Isles 1985a; (8) Isles 1985b; (9) Hübscher and Mundry 1984; (10) Isles 1985c; (11) Mikulášek 1986; (12) Isles 1989; (13) Hübscher et al. 1986; (14) Mikulášek and Šilhán 1988; (15) BBSAG 1987; (16) Hübscher and Lichtenknecker 1988; (17) BBSAG 1988a; (18) BBSAG 1988b; (19) Mikulášek et al. 1992; (20) Hübscher et al. 1989; (21) BBSAG 1989a; (22) Hübscher et al. 1990; (23) BBSAG 1989b; (24) Isles 1992; (25) BBSAG 1990a; (26) Zejda 1995; (27) BBSAG 1990b; (28) De Young et al. 1991; (29) BBSAG 1991; (30) Hübscher et al. 1992; (31) Hübscher et al. 1993; (32) BBSAG 1992a; (33) BBSAG 1992b; (34) Hübscher et al. 1994; (35) BBSAG 1994a; (36) BBSAG 1994b; (37) BBSAG 1995; (38) Mikulášek and Zejda 2002; (39) Šafář and Zejda 2000a; (40) Baldwin and Samolyk 2004; (41) Šafář and Zejda 2000b; (42) Lee et al. 2004; (43) Brát et al. 2007; (44) Nelson 2001; (45) Nelson 2002; (46) BBSAG 2002; (47) Baldinelli and Maitan 2002; (48) Agerer and Hübscher 2002; (49) Zejda 2004; (50) BBSAG 2001; (51) Diethelm 2003; (52) Agerer and Hübscher 2003; (53) Nelson 2003; (54) Nagai 2003; (55) Gürol et al. 2003; (56) Hübscher et al. 2005; (57) Krajci 2005; (58) Hübscher 2005; (59) Diethelm 2004; (60) Maciejewski and Karska 2004; (61) Pribulla et al. 2005; (62) Bíró et al. 2006; (63) Baldwin and Samolyk 2007; (64) Diethelm 2005; (65) Zejda et al. 2006; (66) Hübscher et al. 2006; (67) Nagai 2006; (68) Parimucha et al. 2009; (69) Nagai 2007; (70) Hübscher and Walter 2007; (71) Doğru et al. 2007; (72) Ogloza et al. 2008; (73) Paschke 2007; (74) Nagai 2008; (75) Samolyk 2008a; (76) Samolyk 2008b; (77) Samolyk 2009; (78) Lee et al. 2009; (79) Alton 2013 (present study); (80) Hübscher et al. 2009; (81) Brát et al. 2011; (82) Parimucha et al. 2011; (83) Nagai 2010; (84) Samolyk 2010; (85) Diethelm 2010; (86) Diethelm 2011; (87) Hübscher 2011; (88) Diethelm 2012; (89) Nagai 2012*

Table 4. Near-term recalculated eclipse timing residuals $(ETR)_2$ for BX Peg following simple linear least squares fit of residuals $(ETR)_1$ from reference epoch and cycle number between 2008 July 03 and 2011 Nov 08.

Time of Minimum (HJD–2400000)	*Type*	*Cycle Number*	*$(ETR)_1$[a]*	*$(ETR)_2$*	*Reference**
54650.7799	p	7669	0.00025870	0.00089989	1
54678.4008	s	7767.5	0.00001525	0.00076849	2
54690.4604	s	7810.5	0.00165415	0.00071113	2
54702.6579	p	7854	0.00098420	0.00065310	1
54721.7261	p	7922	0.00078060	0.00056239	3
54736.7282	s	7975.5	0.00053365	0.00049102	4
54736.8681	p	7976	0.00022480	0.00049036	4
54737.7092	p	7979	0.00007170	0.00048635	4
54737.8500	s	7979.5	0.00066285	0.00048569	4
54738.6912	s	7982.5	0.00060975	0.00048168	4
54747.5241	p	8014	0.00036553	0.00043966	5
54751.5906	s	8028.5	0.00074555	0.00042032	5
54752.5719	p	8032	0.00061027	0.00041565	5
54755.5164	s	8042.5	0.00076442	0.00040164	5
54757.3391	p	8049	0.00073270	0.00039297	6
54759.5824	p	8057	0.00068110	0.00038230	5
54759.7225	s	8057.5	0.00058225	0.00038163	4
54760.7033	p	8061	–0.00007970	0.00037697	4
54761.6856	s	8064.5	0.00075835	0.00037230	4
54763.5079	p	8071	0.00029330	0.00036363	5
54766.5923	p	8082	0.00015527	0.00034895	5
54770.5184	p	8096	0.00043080	0.00033028	5
54785.6608	p	8150	0.00024500	0.00025824	4
54786.6426	s	8153.5	0.00058305	0.00025357	4
55000.4587	p	8916	–0.00181320	–0.00076360	7
55000.4587	p	8916	–0.00181320	–0.00076360	7
55000.4590	p	8916	–0.00151320	–0.00076360	7
55057.3837	p	9119	–0.00160630	–0.00103440	8
55061.0300	p	9132	–0.00073640	–0.00105175	9
55061.1705	s	9132.5	–0.00044525	–0.00105241	9
55087.6684	p	9227	–0.00201790	–0.00117848	10
55107.2959	p	9297	–0.00375690	–0.00127186	10
55121.6025	p	9348	0.00154040	–0.00133989	11
55121.7390	s	9348.5	–0.00216845	–0.00134056	11
55146.5572	p	9437	–0.00093490	–0.00145861	10
55383.7904	p	10283	–0.00110910	–0.00258718	12
55481.3719	p	10631	–0.00496870	–0.00305141	13

table continued on next page

Table 4. Near-term recalculated eclipse timing residuals $(ETR)_2$ for BX Peg following simple linear least squares fit of residuals $(ETR)_1$ from reference epoch and cycle number between 2008 July 03 and 2011 Nov 08, cont.

Time of Minimum (HJD–2400000)	*Type*	*Cycle Number*	*$(ETR)_1$[a]*	*$(ETR)_2$*	*Reference**
55481.5166	s	10631.5	–0.00047755	–0.00305207	13
55482.3561	s	10634.5	–0.00223065	–0.00305608	13
55840.5864	p	11912	–0.00549907	–0.00476026	5
55841.7065	p	11916	–0.00715320	–0.00476559	5
55841.5692	s	11915.5	–0.00419102	–0.00476493	5
55842.5498	p	11919	–0.00509963	–0.00476960	5
55842.6907	s	11919.5	–0.00435515	–0.00477026	5
55843.6711	p	11923	–0.00543377	–0.00477493	5
55843.5318	s	11922.5	–0.00455825	–0.00477427	5
55844.6536	s	11926.5	–0.00436905	–0.00477960	5
55849.7021	s	11944.5	–0.00341765	–0.00480361	14
55850.6809	p	11948	–0.00607960	–0.00480828	14
55868.6284	p	12012	–0.00529240	–0.00489366	5
55868.4891	s	12011.5	–0.00442688	–0.00489299	5
55873.5372	s	12029.5	–0.00380882	–0.00491700	5

Note: a. Eclipse Timing Residuals; $(ETR)_1$ from linear elements; (Kreiner 2004) for BX Peg.

** References:; (1) Samolyk 2008b; (2) Parimucha et al. 2009; (3) Samolyk 2009; (4) Lee et al. 2009; (5) Alton 2013 (present study); (6) Hübscher et al. 2009; (7) Brát et al. 2011; (8) Parimucha et al. 2011; (9) Nagai 2010; (10) Samolyk 2010; (11) Diethlem 2010; (12) Diethlem 2011; (13) Hübscher 2011; (14) Diethlem 2012.*

Table 5. Difference in BX Peg light curve magnitude at minimum and maximum light.

Bandpass (Year)	*Min I–Min II*	*Max I–Max II[a]*	*Min I–Max I*	*Min II–Max II*
B (2008)	0.119	0.016	0.724	0.621
V (2008)	0.122	0.009	0.694	0.581
I_c (2008)	0.101	0.007	0.614	0.520
B (2011)	0.199	–0.013	0.794	0.582
V (2011)	0.160	–0.024	0.747	0.563
I_c (2011)	0.101	–0.005	0.650	0.544

Note: a. Measure of asymmetry at maximum light.

Table 6. Spectral classification of BX Peg based upon data from various survey catalogs and present study.

Stellar Attribute	*Tycho-2*	*USNO-B1.0*	*USNO-A2.0*	*All Sky Combined*	*MPOSC3*	*2MASS*	*SDSS-DR8*	*Present Study*
(B–V)	0.871	0.695	0.617	0.764	0.812	0.812	0.766	0.716
Teff[a] (K)	5258	5660	5837	5503	5390	5390	5504	5613
Spectral Class[b]	G9-K0	G6V	G3V	G7-G8V	G9V	G9V	G7-G8V	G7V

Notes: a. Interpolated from Flower (1996). b. Estimated from Harmanec (1988).

Table 7. Absolute and relative system dimensions for BX Peg

Parameter	*Present Study*		*Lee et al. 2009*
	2008	*2011*	
$M_1(M_\odot)$	0.96 (0.059)[a]	0.96 (0.059)	
$M_2(M_\odot)$	0.352 (0.022)	0.356 (0.022)	
$R_1(R_\odot)$	0.9391 (0.0025)	0.9466 (0.0041)	
$R_2(R_\odot)$	0.5971 (0.0013)	0.6081 (0.0014)	
$a(R_\odot)$	1.9717 (0.0029)	1.9735 (0.0042)	
r_1(back)	0.5041 ± 0.0038	0.5084 ± 0.0037	0.5034 ± 0.0012
r_1(side)	0.4762 ± 0.0036	0.4793 ± 0.0035	0.4752 ± 0.0009
r_1(pole)	0.4442 ± 0.0034	0.4465 ± 0.0032	0.4435 ± 0.0007
r_1(volume)	0.4739 ± 0.0033	0.4767 ± 0.0035	0.4755
r_2(back)	0.3293 ± 0.0025	0.3366 ± 0.0024	0.3310 ± 0.0016
r_2(side)	0.2932 ± 0.0022	0.2978 ± 0.0022	0.2946 ± 0.0010
r_2(pole)	0.2807 ± 0.0021	0.2847 ± 0.0021	0.2820 ± 0.0009
r_2(volume)	0.3004 ± 0.0023	0.3047 ± 0.0022	0.3042

Note: *a. Formal error estimates from numerical methods according to Prša and Harmanec (2010; PHOEBE 0.32 manual).*

Table 8. A comparison of synthetic light curve parameters for BX Peg.

Parameter	*Lee et al. 2009 Group 1 Fit*[a]	*Present Study No Spot (2008)*	*Present Study Cool Spot 1 (2008)*	*Present Study No Spot (2011)*	*Present Study Cool Spot 1 (2011)*
T_1 (K)[b]	5532	5520	5520	5520	5520
T_2 (K)[c]	5300 ± 20	5957 ± 15	5858 ± 16	5978 ± 18	5998 ± 15
q (m_2/m_1)[c]	2.6897 ± 0.0045	0.3701 ± 0.0008	0.3669 ± 0.0016	0.3713 ± 0.0046	0.3705 ± 0.0015
A[b]	0.5	0.5	0.5	0.5	0.5
g[b]	0.32	0.32	0.32	0.32	0.32
$\Omega_1 = \Omega_2$[c]	6.135 ± 0.010	2.5804 ± 0.0006	2.586 ± 0.0036	2.589 ± 0.0013	2.578 ± 0.0055
i°[c]	87.693 ± 0.095	87.53 ± 0.89	88.30 ± 1.13	89.27 ± 0.35	88.92 ± 0.48
$A_{S1} = T_{S1} / T$[d]	0.828 ± 0.050	—	0.80 ± 0.01	—	0.83 ± 0.01
Θ_{S1} (spot co-latitude)[d]	66.6 ± 2.1	—	90 ± 3.2	—	90 ± 7.7
φ_{S1} (spot longitude)[d]	142.7 ± 0.4	—	143 ± 1.7	—	292 ± 3
r_{S1} (angular radius)[d]	14.1 ± 0.1	—	12.9 ± 0.13	—	15.3 ± 0.23
$\chi 2$ (B)[e]	—	0.036536	0.031770	0.023576	0.019429
$\chi 2$ (V)	—	0.054780	0.037238	0.030995	0.021960
$\chi 2$ (I_c)	—	0.140966	0.109502	0.096506	0.080949

Notes: a. Parameters and error reported by Lee et al. (2009) using m_1/m_2. b. Fixed during DC. c. Error estimates from heuristic scanning with PHOEBE *0.31a (Prša and Zwitter 2005). d. Error estimates from* WDWINT *v5.6a (Nelson 2009). e. $\chi 2$ from* PHOEBE *0.31a (Prša and Zwitter 2005).*

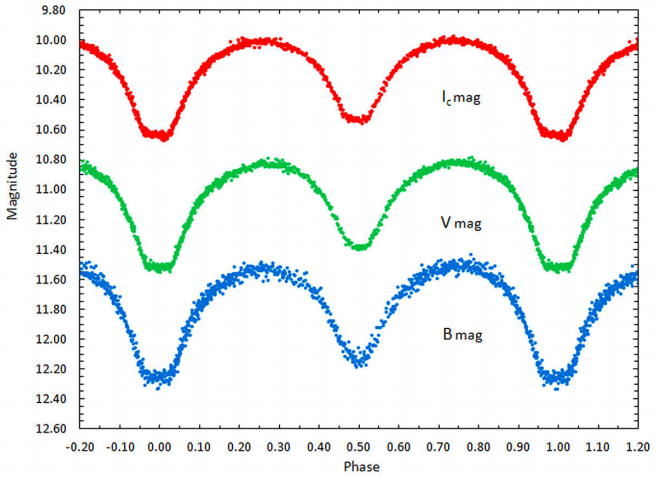

Figure 1. Folded CCD light curves for BX Peg produced from photometric data obtained between October 8 and October 31, 2008. The top (I_c), middle (V), and bottom (B) curves shown above were reduced to MPOSC3-based catalogue magnitudes using MPO CANOPUS.

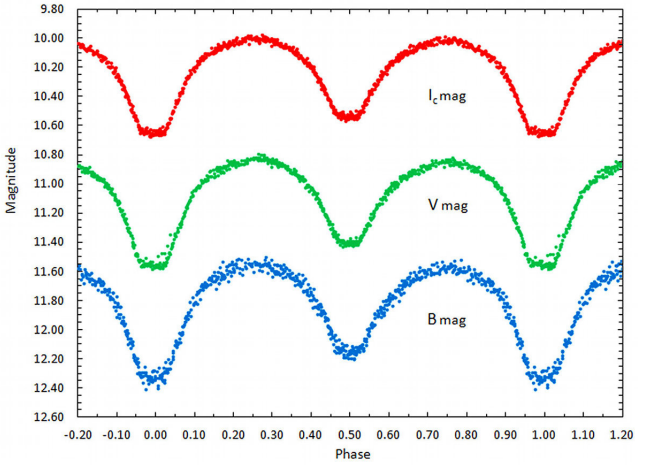

Figure 2. Folded CCD light curves for BX Peg produced from photometric data obtained between October 6 and November 8, 2011. The top (I_c), middle (V), and bottom (B) curves shown above were reduced to MPOSC3-based catalogue magnitudes using MPO CANOPUS.

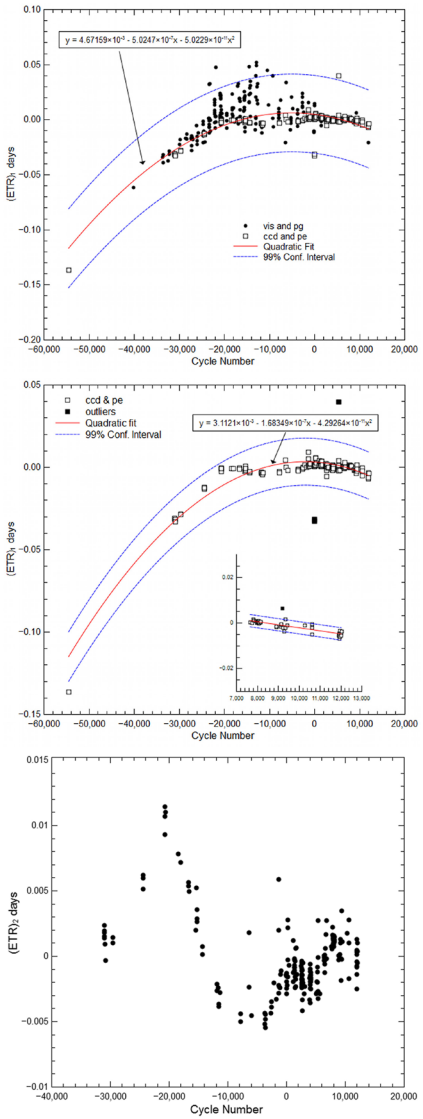

Figure 3. Non-linear regression fit (top) from visual, pg, PE, and CCD times of minimum (1960–2011) for BX Peg using a quadratic expression weighted 8:1 with respect to instrumental and non-instrument readings. The middle plot shows quadratic fit only from the CCD and PE times of minimum. The inset graph shows a straight-line fit and 99% confidence intervals of ET data between 2008 and 2011 which were used to calculate a near term linear ephemeris for BX Peg. Residuals $(ETR)_2$ from the quadratic fit of instrumental (CCD and PE) eclipse timings are shown in the bottom panel.

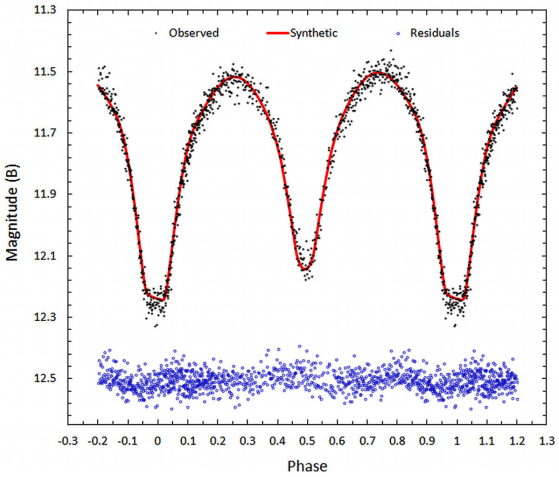

Figure 4. Synthetic fit of light curve (B mag.) for BX Peg collected at UO during 2008 using Roche model parameters (T_1, T_2, i, q, Ω, and cold spot) identical to those reported by Lee *et al.* (2009). Residuals are offset by a constant value to keep the y-axis on scale.

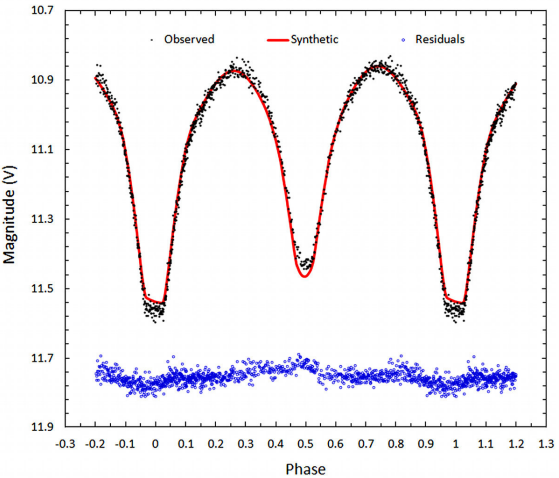

Figure 5. Synthetic fit of light curve (V mag.) for BX Peg collected at UO during 2008 using Roche model parameters (T1, T2, i, q, Ω, and cold spot) identical to those reported by Lee *et al.* (2009). Residuals are offset by a constant value to keep the y-axis on scale.

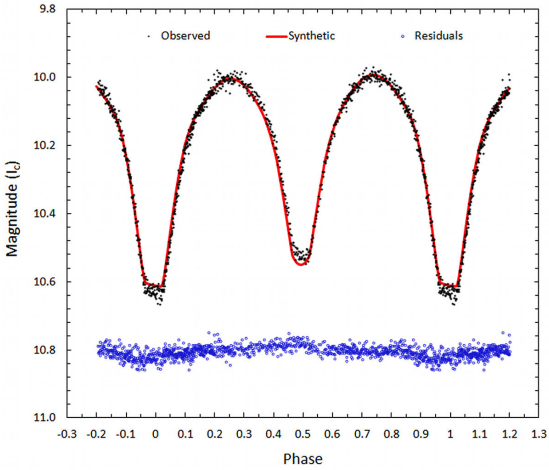

Figure 6. Synthetic fit of light curve (I_c mag.) for BX Peg collected at UO during 2008 using Roche model parameters (T_1, T_2, i, q, Ω, and cold spot) identical to those reported by Lee *et al.* (2009). Residuals are offset by a constant value to keep the y-axis on scale.

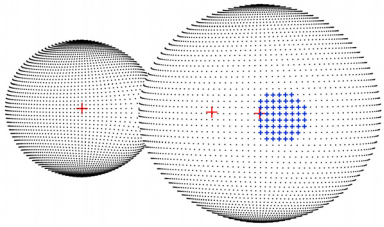

Figure 7. 3-D spatial representation (phase = 0.10) of BX Peg during October 2008 with cool spot positioned on the more massive star visible to the viewer during and slightly after Min I.

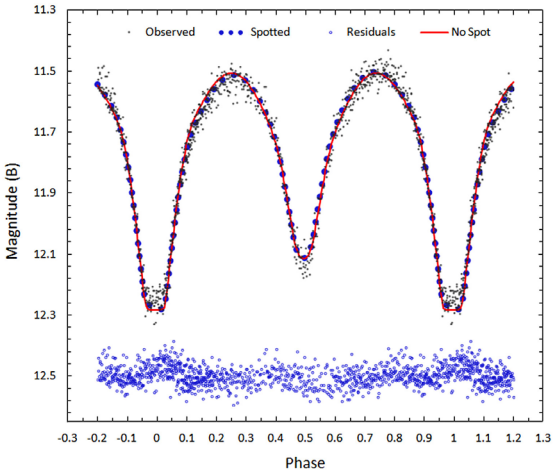

Figure 8. Synthetic fits of BX Peg light curve (B mag.) collected at UO during 2008 using an unspotted (solid-line) and a spotted (dotted-line) Roche model which incorporates a cool spot on the more massive star. Spotted residuals are offset by a constant value to keep the y-axis on scale.

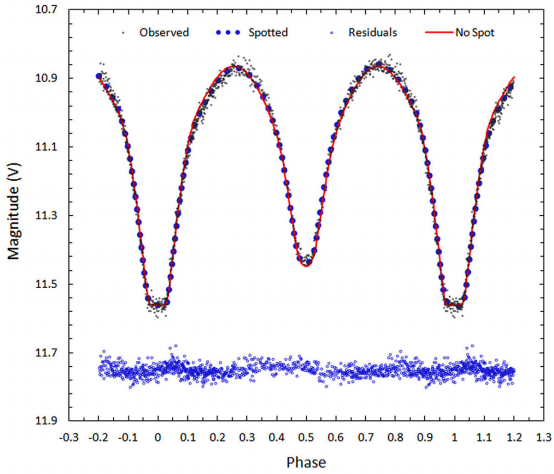

Figure 9. Synthetic fit of light curve (V mag.) for BX Peg collected at UO during 2008 using an unspotted (solid-line) and spotted (dotted-line) Roche model which incorporates a cool spot on the more massive star. Spotted residuals are offset by a constant value to keep the y-axis on scale.

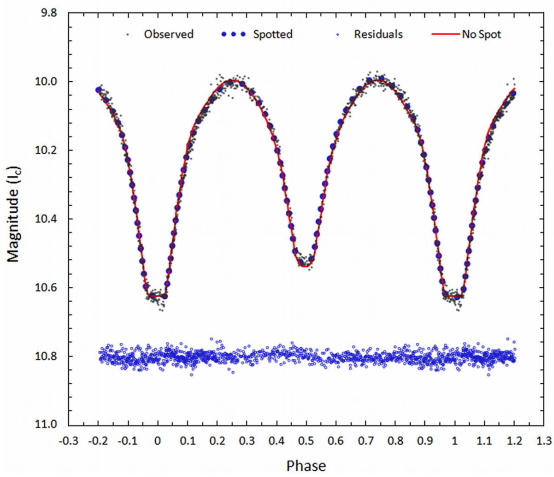

Figure 10. Synthetic fit of light curve (I_c mag.) for BX Peg collected at UO during 2008 using an unspotted (solid-line) and spotted (dotted-line) Roche model which incorporates a cool spot on the more massive star. Spotted residuals are offset by a constant value to keep the y-axis on scale.

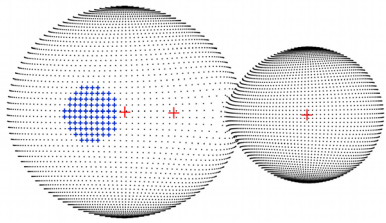

Figure 11. 3-D spatial model (phase = 0.63) of BX Peg between October and November 2011 with a cool spot positioned on the more massive star which diminishes brightness during Max II.

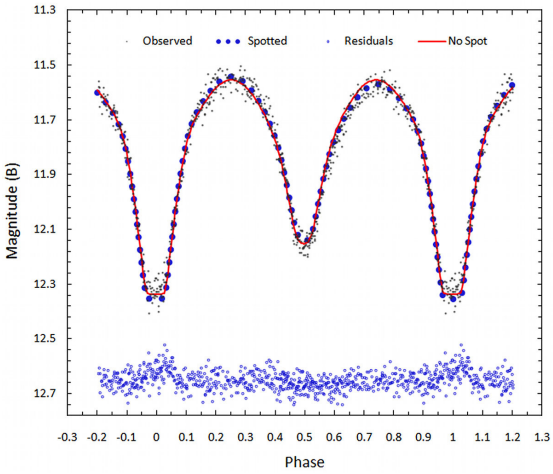

Figure 12. Synthetic fit of light curve (B mag.) for BX Peg collected at UO during 2011 using an unspotted (solid-line) and spotted (dotted-line) Roche model which incorporates a cool spot on the more massive star. Spotted residuals are offset by a constant value to keep the y-axis on scale.

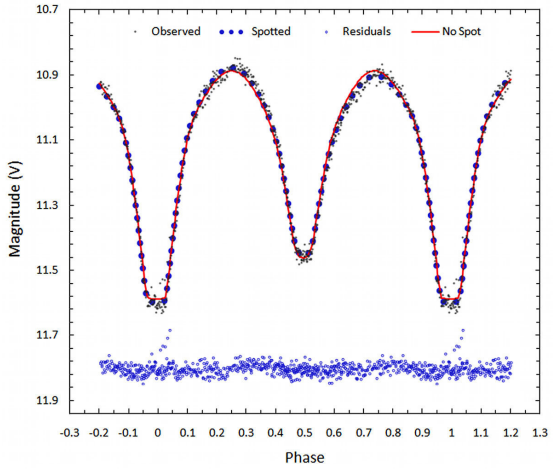

Figure 13. Synthetic fit of light curve (V mag.) for BX Peg collected at UO during 2011 using an unspotted (solid-line) and spotted (dotted-line) Roche model which incorporates a cool spot on the primary star. Spotted residuals are offset by a constant amount in order to keep the y-axis on scale.

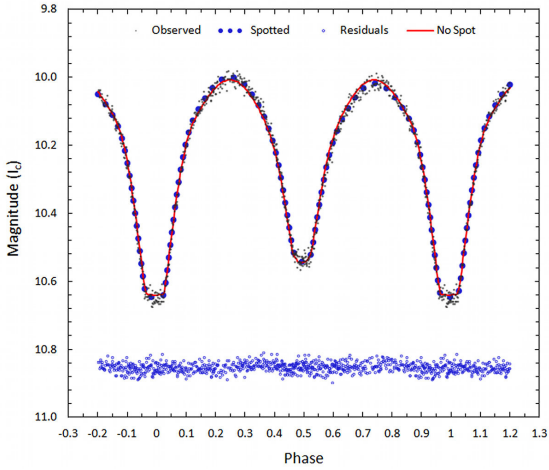

Figure 14. Synthetic fit of light curve (I_c mag.) for BX Peg collected at UO during 2011 using an unspotted (solid-line) and spotted (dotted-line) Roche model which incorporates a cool spot on the primary star. Spotted residuals are offset by a constant amount in order to keep the y-axis on scale.